Tungsten laminates made of ultrafine-grained (UFG) tungsten foil — Ageing of tungsten–titanium (W–Ti) laminates

Jens Reiser [a,*], Peter Franke [a], Tobias Weingärtner [a], Jan Hoffmann [a], Andreas Hoffmann [b], Michael Rieth [a]

[a] Karlsruhe Institute of Technology, Institute for Applied Materials, Hermann-von-Helmholtz-Platz 1, 76344 Eggenstein-Leopoldshafen, Germany
[b] PLANSEE SE, 6600 Reutte, Austria

ARTICLE INFO

Keywords:
Ageing
Auger electron spectroscopy (AES)
Diffusion mechanism
Ductility
Simulation

ABSTRACT

Through the synthesis of a tungsten laminate made of ultrafine grained (UFG) tungsten foils, a UFG bulk material can be made that retains the ductility and toughness of the tungsten foils. Considering tungsten laminates as a structural material the ageing behaviour is of utmost importance.
In this paper we analyse and discuss the ageing behaviour of tungsten laminates produced by diffusion bonding using a titanium (Ti) interlayer. The evolution of the mechanical properties (Charpy impact, hardness) and the evolution of the microstructure during annealing at 1000 °C for 10 h, 100 h, and 1000 h in vacuum are studied. The calculated Ti W phase diagram, as well as the calculated interdiffusion coefficients and interdiffusion profiles, significantly relate to the understanding of the evolution of the W Ti interface. Comparison of Auger electron spectroscopy (AES) and scanning electron microscope (SEM) analyses with the simulated diffusion data provides an in depth understanding of the diffusion mechanisms and the evolution of the microstructure. The elucidation of the diffusion mechanisms of W Ti laminates will advance several research fields such as the production of UFG bulk material and the synthesis of advanced fracture toughness test samples.

1. Introduction

Tungsten (W) is the metal with the highest melting point of all metals (3422 °C) [1] and should therefore be an excellent candidate for structural high temperature applications. One disadvantage that im pedes the use of tungsten for structural parts is its low room temperature (RT) fracture toughness, K_{IC}, and its high brittle to ductile transition temperature (BDTT) [2]. However, for tungsten in the shape of a severe cold rolled thin foil the situation appears rather different.

Tungsten foil in the as rolled (and stress relieved) condition has exceptional mechanical properties in terms of ductility [3], toughness [4,5], and brittle to ductile transition (BDT) [6].

Wei and Kecskes [3] evaluated the tensile behaviour of commercially pure tungsten as a function of low temperature rolling. They observed that rolling below the nominal recrystallisation temperature of 1523 K (1250 °C) concomitantly enhances the strength and ductility of tungsten. Furthermore, Pippan [4,5] assessed the fracture toughness of pure tungsten foil with a thickness of 160 μm in the as rolled condition. He determined a RT fracture toughness, K_{IQ}, of 70 MPa $m^{1/2}$ in the L T direction and of 55 MPa $m^{1/2}$ in the T L direction (more details on the two letter code can be found in Ref. [7]). Finally Németh et al. [6] evaluated the nature of the BDT of annealed coarse grained and as received ultrafine grained (UFG) tungsten foil. For the UFG tungsten foil they determined a BDTT of about 77 K, assuming that the BDT in UFG tungsten is controlled by the glide of edge dislocations.

These exceptional mechanical properties might be attributed both to the positive response of tungsten to cold rolling and to the ultrafine grained microstructure of the tungsten foil.

One of our approaches to making tungsten ductile makes use of the exceptional properties of UFG tungsten foils. These foils are the starting point of the synthesis of a tungsten foil laminate, a multi layer material (Fig. 1) [8]. Through the synthesis of a tungsten laminate, a UFG bulk material can be made that retains the ductility and toughness of the tungsten foils. Furthermore, by coiling up and joining, tungsten laminate pipes can be produced (Fig. 1) [5]. The technical maturity of these tungsten laminate pipes has been proven by high heat flux tests performed at the Plataforma Solar de Almería, Spain, and at the Max Planck Institute for Plasma Physics, Garching, Germany [5].

Obviously, the mechanical properties of a tungsten foil laminate depend on the joining technology and the interlayer used. In this paper we assess the properties of tungsten laminates produced by diffu sion bonding using a titanium (Ti) interlayer. As tungsten foil laminates are intended to be used for structural high temperature applications the evolution of the mechanical properties during annealing is of utmost interest. The change of the mechanical properties during annealing is

* Corresponding author at: Karlsruhe Institute of Technology (KIT), Institute for Applied Materials (IAM), Hermann-von-Helmholtz-Platz 1, 76344 Eggenstein-Leopoldshafen, Germany.
E-mail addresses: jens.reiser@kit.edu (J. Reiser), peter.franke@kit.edu (P. Franke), tobias.weingaertner@kit.edu (T. Weingärtner), j.hoffmann@kit.edu (J. Hoffmann), andreas.hoffmann@plansee.com (A. Hoffmann), michael.rieth@kit.edu (M. Rieth).

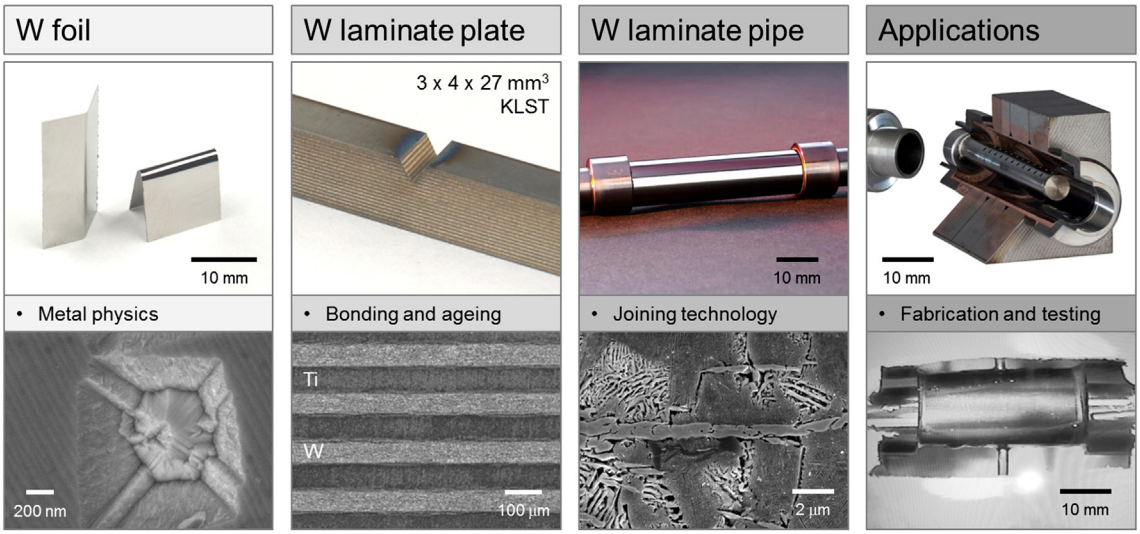

Fig. 1. Overview of the material system 'W foil laminates'.

caused by both the recrystallisation of the tungsten foils and the evolution of the W Ti interface.

The following chapters therefore address these questions.

(1) What is the evolution of the mechanical properties (Charpy impact, hardness) and the evolution of the microstructure during annealing for 10 h, 100 h, and 1000 h at 1000 °C in vacuum?
(2) What are the diffusion mechanisms in W Ti laminates?
(3) How can Auger electron spectroscopy (AES) analyses as well as thermodynamic and kinetic calculations contribute to an in depth understanding of the evolution of the W Ti interface?
(4) Is there a correlation between the change in the mechanical properties and the change in the microstructure?

The paper is organised as follows: to provide an overview, three synthesis strategies for a tungsten foil laminate are briefly introduced and discussed in the following section. Thereafter the synthesis of the W Ti laminates and the ageing conditions are described. After that, the analytical and experimental methods such as AES and Charpy impact tests are presented. Afterwards, the results of the simulation of the Ti W phase equilibria and the diffusion in W Ti laminates are displayed. Finally, the results of the simulation, microstructural analyses and mechanical tests are discussed, and an in depth explanation of the diffusion mechanisms in W Ti laminates is given.

2. Background: synthesis strategies for tungsten foil laminates

For the tungsten laminate synthesis we pursue three approaches. The first one makes use of a high melting interlayer, such as vanadium ($Tm = 1910$ °C [1]) or titanium (melting temperature, $Tm = 1668$ °C [1]) which is the object of this work. Such laminates are predestined to elucidate diffusion mechanisms in tungsten [9,10].

The second synthesis strategy consists in the production of tungsten laminates without any interlayer at all. By diffusion boning of several layers of tungsten foil, this approach has been demonstrated successful ly. Lison [11,12] provided comprehensive explanations on how to join tungsten and he recommended detailed parameters for direct diffusion bonding of tungsten to tungsten without any interlayer at all (2200 °C, 20 MPa, 15 min [11] and 1300 °C 2000 °C, 2 20 MPa [2]). In order to reduce the bonding temperature and bonding time, the activation of the tungsten foil surfaces by several atom layers of specific elements like e.g. titanium is an option [12].

With the third approach we follow the recommendation by Pippan, which is to produce tungsten laminates with copper (Cu) interlayers smaller than 1 µm. Copper has a melting temperature of 1084.62 °C [1], and the copper tungsten phase diagram shows no sol ubility of tungsten in liquid copper [13,14]. This results in excellently sharp interfaces. By decreasing the copper interlayer thickness well below 1 µm, a dimensional size effect is realised. Gliding dislocations in the copper phase face sharp tungsten interfaces as well as impen etrable tungsten surfaces and are thus forced to 'channel'. It is expect ed that this dislocation channelling enhances the strength of the copper interlayer significantly [15,16]. Such W Cu laminates combine two types of size effects. These are on the one hand microstructural size effects owed to the UFG microstructure of the tungsten foil, and on the other hand dimensional size effects (SE) owed to the small thickness of the copper interlayer. This type of material is referred to as SE^2 material. In general W Cu laminates can contribute to questions about the mechanical strength of thin films [15,16] and dimensional size effects of nanoscaled multi layered copper based composites [17] such as accumulative roll bonded copper niobium composites [18,19], or copper chromium [20], copper nickel [17, 21], and copper gold [20] multilayer material systems.

A further trail is the synthesis of W Cu laminates made of recrystal lised tungsten foils. Tensile tests on recrystallised tungsten foils have proved the mechanism of dislocation annihilation on the free surface, resulting in an enhanced plastic deformability [22]. Furthermore, it has been shown that the mechanism of dislocation annihilation also takes place on a W Cu interface. Especially with regard to the use of W Cu laminates for nuclear fusion applications, W Cu laminates made of recrystallised tungsten foil might be an interesting option.

All laminate synthesis strategies have to address the issue of how to deal with the tungsten oxide layers. Efficient ways to remove tungsten oxides like tungsten trioxide (α WO_3), β tungsten oxide ($WO_{2.9}$, ($W_{20}O_{58}$)), β tungsten oxide ($WO_{2.72}$, ($W_{18}O_{49}$)), and tungsten dioxide (WO_2) are either by plasma etching prior to the physical vapour depo sition (PVD) of the interlayer or by annealing in vacuum prior to the brazing or diffusion bonding process [2,23]. The latter approach is what we make use of in this work. Another approach to dealing with the oxides makes use of tolerating the oxide layers and to perform the laminate synthesis by an impulse pressuring diffusion bonding process. The idea is that impulse pressuring breaks the oxide films, leading to an improved bonding interface [24].

Beside diffusion mechanisms and the issue of oxide layers, the lam inate synthesis strategy has to be discussed against the background of possible mechanical properties. Here it is worthwhile to consider the

impact of residual stresses as well as of ongoing crack deflection at the interfaces on the damage tolerance of the laminate.

3. Materials and experimental methods

This chapter is divided into three parts. In the first part the micro structure of the tungsten foil, the synthesis of the W Ti laminates and the ageing conditions are described. After that, details on the AES analyses are displayed, and finally the experimental set up for the Charpy impact tests is presented.

3.1. Synthesis of W Ti laminates and ageing conditions

The tungsten material used for the synthesis of W Ti laminates is technically pure tungsten foil (>99.97 wt.% W) with a thickness of 100 μm. This commercially available foil was manufactured by PLANSEE SE by a powder metallurgical route consisting of sintering and hot and cold rolling. The impurity concentrations which PLANSEE SE guarantees not to exceed are shown in Table 1.

Because of the high degree of cold rolling the tungsten foil possesses a pancake shaped microstructure with elongated grains in both the T and L direction. In the S direction the grain size distribution ranges mainly between 0.2 and 0.5 μm [6,25]. The rolled foil has a pronounced rotated cube texture, {001}<110>, and contains a high percentage of low angle subgrains, which is well known in severe cold rolled metals. With regard to the temperature stability of the microstructure, polygonisation is meant to start at 900 °C whereas nucleation formation does not take place. Recrystallisation in terms of migration of grain boundaries is expected to start at 1200 °C [25]. Because of the exceptional recrystallisation behaviour of the tungsten foil, the sharp rotated cube texture in the as received condition becomes even more pronounced with annealing.

The titanium material used for the synthesis of the W Ti laminates is commercially available pure titanium foil (>99.6 wt.% Ti), also with a thickness of 100 μm. The typical impurity concentrations according to the supplier are shown in Table 1. The microstructure of the titanium foil in the as received condition shows equiaxed grains with a mean grain size of 50 μm.

The synthesis of the W Ti laminates was as follows: 20 layers of tungsten foil and 19 layers of titanium foil were put on each other alter nately. This stack of 39 foils was then put in an electro mechanical universal test device (ZWICK 100) modified and combined with a vacuum chamber and a furnace (MAYTEC). The stack of foils was heated up to 900 °C in a high vacuum (1×10^{-5} mbar 5×10^{-5} mbar). Because of the low oxygen partial pressure some tungsten oxides are expected to be volatile. The stack of foils was diffusion bonded for 1 h. The furnace cooled down to RT at a cooling rate of 450 K/h. The material condition directly after cooling down is referred to as 'as produced' in this paper.

The ageing conditions were as follows: the as produced W Ti laminates were sealed in vacuum by glass coquilles (1×10^{-5} mbar 5×10^{-5} mbar) and were annealed for 10 h, 100 h, and 1000 h at 1000 °C. The samples cooled down to RT at a cooling rate of 100 K/h.

The microstructural analyses and experiments described in this paper were carried out on W Ti laminates in four conditions. These are the (i) as produced condition, as well as the annealed conditions like (ii) 10 h, (iii) 100 h and (iv) 1000 h at 1000 °C in vacuum. An image of a W Ti laminate can be seen in Fig. 1, and Fig. 2 gives an impression of the microstructure and evolution of the interface.

From the as produced and annealed W Ti laminates, Charpy impact test samples of KLST type (27 mm × 3 mm × 4 mm, 1 mm notch depth, 0.1 mm notch root radius, and 22 mm span) were cut by spark erosion. The samples cut represent the L S direction.

Table 1
Impurity concentration of the W and Ti foil used. The first line shows the maximum concentration of selected elements in W which PLANSEE SE guarantees not to exceed. The second line shows the typical concentration of selected elements in the Ti foil.

Element	C	H	N	O	Si
W: guaranteed analyses (max.), μg/g	30	5	5	20	20
Ti: typical analyses, μg/g	300	60	150	2000	300

3.2. Auger electron spectroscopy

A Physical Electronics PHI 680 Xi Field Emission Scanning Auger Nanoprobe was used for AES. The analyses were performed with 10 keV acceleration voltage and 20 nA beam current for the electron beam. The beam size was close to 24 nm. The sample was tilted 30° from surface normal to electron gun during acquisition. An argon (Ar) ion beam with an ion current of 500 nA was used for sputter etching. To remove the carbon (C) and oxygen (O) contaminants from the surface and to make the grain structure visible, a 15 minute period of sputter etching was applied. During data acquisition, a continuous sputter etching setting with very low ion acceleration was used to prevent a redeposition of contaminations out of the vacuum.

For quantitative measurements in AES, peak to peak height measurements from the derivative spectra were used. The accuracies of such measurements are typically around ±20%. To improve the measurement accuracy, the produced W Ti laminates were first quanti fied precisely by a Camebax Microbeam electron probe microanalysis (EPMA) with a beam size of about 1 μm. The EPMA analyses were followed by spectral AES measurements for the determination of the sensitivity factors. For both methods, measurement areas of ca. 10 μm × 10 μm were placed in the middle of a tungsten layer and a titanium layer. With the data achieved in this way, the laminate samples can be used as calibration standards for further AES analyses. These data were used to converge the AES sensitivity factors by means of an approximation algorithm. The calculated factors were verified by comparing them with other factors from older measurements and by checking the plausibility of the resultant element contents of the refer ence materials. Thus, it can be shown that the measurement accuracy of the AES data in comparison with that of the EPMA data for tungsten contents from about 6 at.% in titanium was ±10%. For high level contents of titanium, the accuracy was ±1%. For AES data reduction, the following sensitivity factors were used: Ti (at 421 eV): 0.182; W (at 182 eV): 0.241.

3.3. Charpy impact tests

Instrumented Charpy impact tests were performed according to the DIN EN ISO 148 1 (2011) and DIN EN ISO 14556 (2006) standards. These standards describe small size specimens with dimensions of 27 mm × 3 mm × 4 mm, 1 mm notch depth, 0.1 mm notch root radius, and 22 mm span (KLST type sample).

The Charpy impact test device is designed in a drop weight style. To avoid oxidation, the whole Charpy testing machine is placed inside a vac uum vessel which operates at typical pressures of about 1×10^{-3} mbar. The specimens are heated up together with the support which allows precise test temperature control. For more technical details of the Charpy impact test device the reader is referred to Ref. [26].

The Charpy impact test results display the dissipated energy plotted against the test temperature. In the study presented, one sample for each laminate condition and test temperature was tested.

4. Simulation of phase equilibria and diffusion in W–Ti laminates

The discussion of the evolution of the W Ti interface during diffusion bonding and ageing has to take into account both the thermo dynamic and the kinetic properties of the W Ti system. Therefore the following chapter focuses on the simulation of the phase diagram of

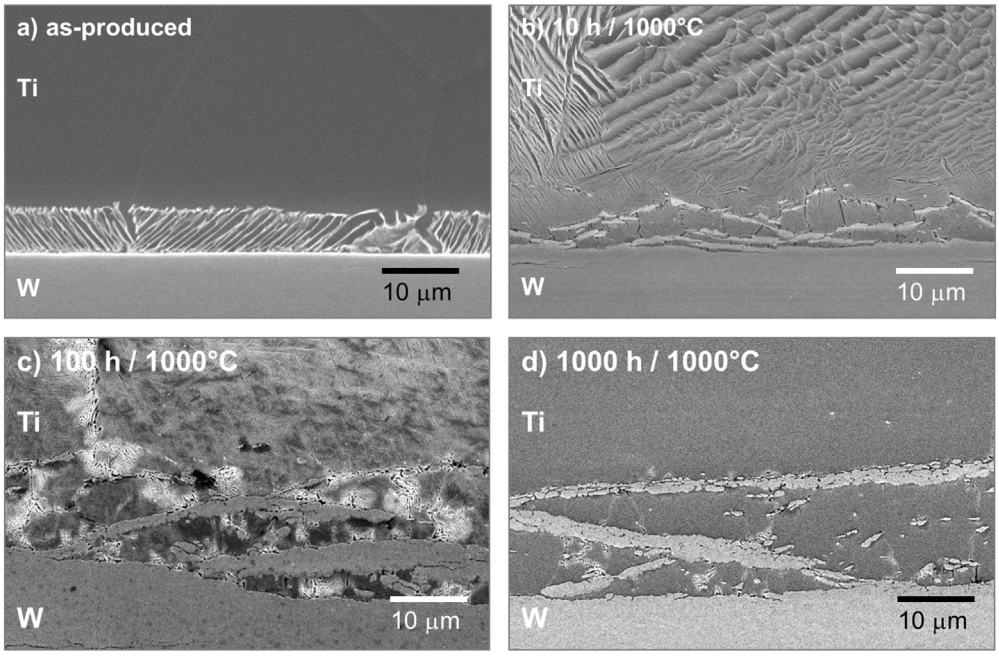

Fig. 2. Scanning electron microscope (SEM) analyses of the W–Ti interface in the four conditions analysed in this paper. These are (i) as-produced, (ii) annealed for 10 h at 1000 °C, (iii) annealed for 100 h at 1000 °C and (iv) annealed for 1000 h at 1000 °C.

the Ti W system as well as on the simulation of diffusion in W Ti laminates.

4.1. Phase equilibria

While tungsten is stable in the body centred cubic (bcc) crystal structure up to its melting point, titanium has two stable modifications, hexagonal α Ti at lower temperatures and bcc β Ti above 882 °C. The phase diagram shown in Fig. 3 demonstrates that titanium and tungsten can form continuous solid solutions with bcc structure at temperatures above 1213 °C. Below this temperature, a miscibility gap separates Ti rich and W rich solutions from each other. The heat treatments performed in this work are located in the temperature range of this miscibility gap. Below the monotectoid temperature of 746 °C the W rich bcc alloys are in equilibrium with hexagonal titanium containing only negligible amounts of tungsten. The phase diagram presented in Fig. 3 has been calculated with the thermodynamic dataset of Saunders [27]. This dataset is also used in the diffusion calculations in order to provide

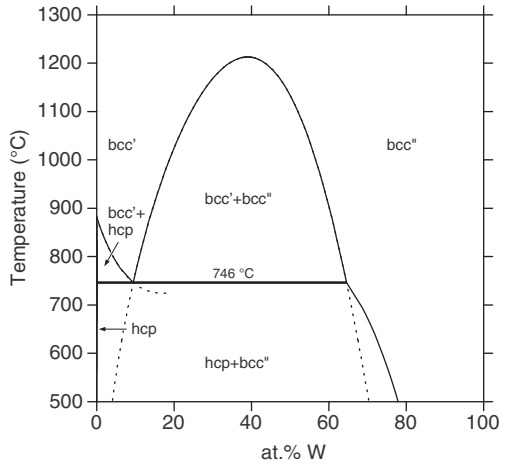

Fig. 3. Phase diagram of the Ti–W system in the sub-solidus range. The dotted lines represent the metastable extensions of the phase boundaries.

the equilibrium concentrations at phase boundaries as well as the driving forces for the diffusional transformations.

4.2. Diffusion data

In addition to the thermodynamic data the kinetics of diffusion controlled phase transformations is determined by interdiffusion coefficients which are dependent on the temperature and the alloy composition.

The interdiffusion process is simulated with the software package DICTRA [28] which can handle diffusion controlled phase transformations with moving phase boundaries in multicomponent systems. In the DICTRA programme the interdiffusion coefficients are calculated from mobilities of the diffusing species and thermodynamic factors [28]. The mobilities of pure elements are closely related to their self diffusion coefficients while in very dilute solution they are closely related to the respective impurity diffusion coefficients. In the present case of diffusion in W Ti alloys the required mobility parameters have been evaluated from several sources. The self diffusion of titanium in bcc Ti was investigated by Pontau and Lazarus [29]. The impurity diffusion of titanium in tungsten was studied recently by Klotsman et al. [30]. The self diffusion of tungsten in tungsten was examined by Arkhipova et al. [31] and impurity diffusion coefficients of tungsten in bcc Ti were reported by Pavlinov [32].

The resulting interdiffusion coefficients in W Ti alloys are shown in Fig. 4 as a function of the W contents for the two temperatures used in the heat treatment of the present experiments, 900 °C and 1000 °C, respectively. In the limit of infinite dilution the interdiffusion coefficient approaches the impurity diffusion coefficient of tungsten in titanium (intercept with the left ordinate in Fig. 4) and of titanium in tungsten, respectively (right intercept in Fig. 4). In the composition range of the miscibility gap the interdiffusion coefficients are not shown in Fig. 4. Since the interdiffusion coefficients become negative within the spinodal range they cannot be displayed on a logarithmic scale. However, the alloy compositions in the W Ti laminates of our experiments are always between pure titanium and the Ti rich boundary of the miscibility gap in the case of the titanium foils and between pure tungsten and the W rich boundary of the miscibility gap in the case of the tungsten foils.

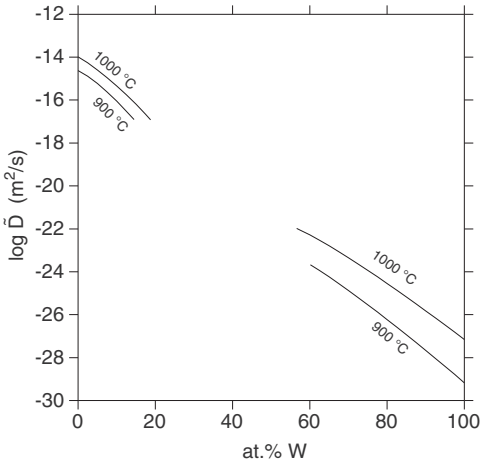

Fig. 4. Composition-dependent interdiffusion coefficient in the bcc phase of the Ti–W system at 900 °C and 1000 °C.

4.3. Simulation of diffusion in W Ti laminates

For the simulation of the diffusion process during the heat treatments of the W Ti laminates (synthesis at 900 °C, annealing at 1000 °C), the following set up was used. Since the laminates consist of alternating layers of titanium and tungsten sheets, each with a thickness of 100 μm, the calculations were confined for symmetry reasons to a range starting at the middle of a titanium sheet and ending in the middle of an adjacent tungsten sheet. Since both metals are practically pure, the initial concentration profile of tungsten in the sheets is initially given by a step function with the jump denoting the interface located at the position of 50 μm. In the simulation the diffusion couple was held at a temperature of 900 °C for a period of 1 h followed by another time interval of 1000 h at 1000 °C. In the simulation the respective tempera tures were imposed immediately on the diffusion couple without finite heating or cooling velocities and without thermal gradients. In Fig. 5 the resulting concentration profile of tungsten is shown along a path from the centre of the titanium sheet to the centre of the tungsten sheet after various simulation times. It can be seen that tungsten diffuses into the titanium sheet whereas the opposite process of titanium enter ing into the tungsten sheet is not visible. As a result of the conservation of mass the interface between the metal sheets is displaced towards the shrinking tungsten sheet. During the diffusion simulation, local equilib rium is assumed at the interface which means that the miscibility gap between the Ti rich and the W rich alloys determines the concentration jump at the interface. Since tungsten develops an extended diffusion profile in the Ti rich sheet the saturation concentration of tungsten in titanium can be compared easily with the corresponding value given by the miscibility gap in the phase diagram. However, the correspond ing equilibrium concentration on the W rich side of the interface cannot be resolved because here the concentration profile is very steep in close vicinity to the interface so that it cannot be distinguished from the vertical concentration jump at the interface. The vast differences in the shapes of the concentration profiles on either side of the interface are caused by the strong concentration dependence of the interdiffusion coefficients shown in Fig. 4. On the Ti rich side of the interface the inter diffusion coefficient is five orders of magnitude higher than that on the W rich side. Moreover, the short scaled interdiffusion profile which is formed on the W rich side in the vicinity of the interface is immediately consumed because the interface moves towards the W rich side, transforming a layer of W rich phase into a layer of Ti rich phase. Therefore, the tungsten sheets remain practically pure whereas the titanium sheets become increasingly enriched with tungsten as the time of the heat treatment is prolonged, as shown in Fig. 6.

The position of the interface as a function of time is shown in Fig. 6. Synonymously it denotes half of the thickness of the Ti rich sheets or as a complement to 100 μm it denotes half of the tungsten sheet thickness. The displacement resulting from the first annealing for 1 h at 900 °C (synthesis of the W Ti laminates) cannot be seen at this scale of the diagram. The calculated interface positions after the experimental annealing times at 1000 °C are indicated in the diagram.

5. Results and discussion

This chapter is organised as follows: first the evolution of the micro structure and in particular the evolution of the W Ti interface is displayed by means of AES and SEM analyses. The results of the micro structural analyses are discussed in light of the thermodynamic and the kinetic properties of the W Ti system and are compared with the results of the simulation of diffusion. Finally, the evolution of the Charpy impact properties and hardness are presented and correlated with the evolution of the microstructure.

5.1. Microstructure after ageing

During manufacturing of the W Ti laminates interdiffusion process es proceed within the foils followed by certain phase transformations in the subsequent cooling stages. During the diffusion bonding at 900 °C as well as during the annealing at 1000 °C the stack of foils is located in the region of the phase diagram above the monotectoid temperature but

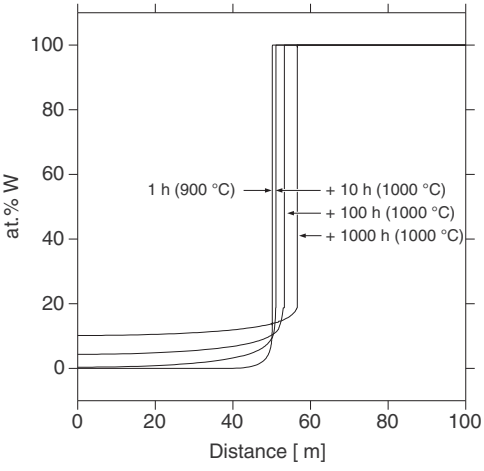

Fig. 5. Calculated interdiffusion profiles in W–Ti laminates after selected times of heat treatment (synthesis at 900 °C, annealing at 1000 °C).

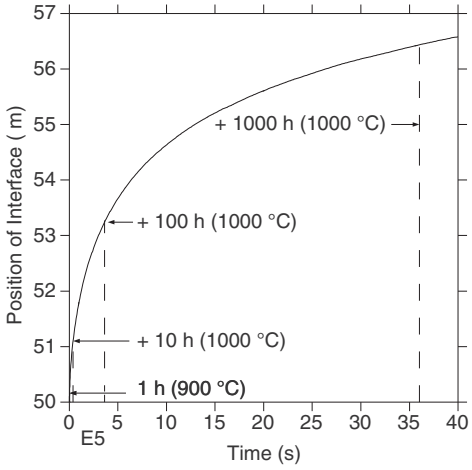

Fig. 6. Calculated interface position between the titanium and tungsten sheets during the heat treatment.

within the range of the miscibility gap in the bcc solid solution. Here, tungsten can dissolve in the titanium sheets up to a tungsten concentra tion of 19 at.% which is established at the interface between the titanium and tungsten foils. With increasing distance from this interface the tungsten concentration decreases to lower levels. In the initial stages of the manufacturing process the interior of the titanium sheets is practically free of tungsten and only in the vicinity of the interface to the tungsten sheet a narrow diffusion zone exists which gradually widens with increasing diffusion time. Therefore, in the initial stages the titanium alloy in the diffusion zone is in the hypo monotectoid com position range except for a nano scaled layer directly at the interface.

In Fig. 7a the microstructure in the vicinity of an interface between a titanium and a tungsten foil is shown after diffusional bonding at 900 °C and furnace cooling at a rate of 450 K/h. The titanium foil has transformed from the bcc high temperature modification into the hexagonal low temperature modification. However, the phase diagram reveals that the solubility of tungsten in hcp Ti is practically negligible. Therefore, the excess amount of tungsten has to be expelled from the transforming crystals and a microstructure of Widmanstätten type is formed in the range of the interdiffusion zone. These observations are in line with the results of other authors [9,10]. The width of the Widmanstätten plates is so narrow that tungsten can still diffuse to the interface of the plates at the moderate cooling velocities of the furnace cooling. At the surface of the Widmanstätten plates a thin layer of bcc (Ti,W) alloy is formed or small particles precipitate. The composition of these precipitates is expected to be given by the

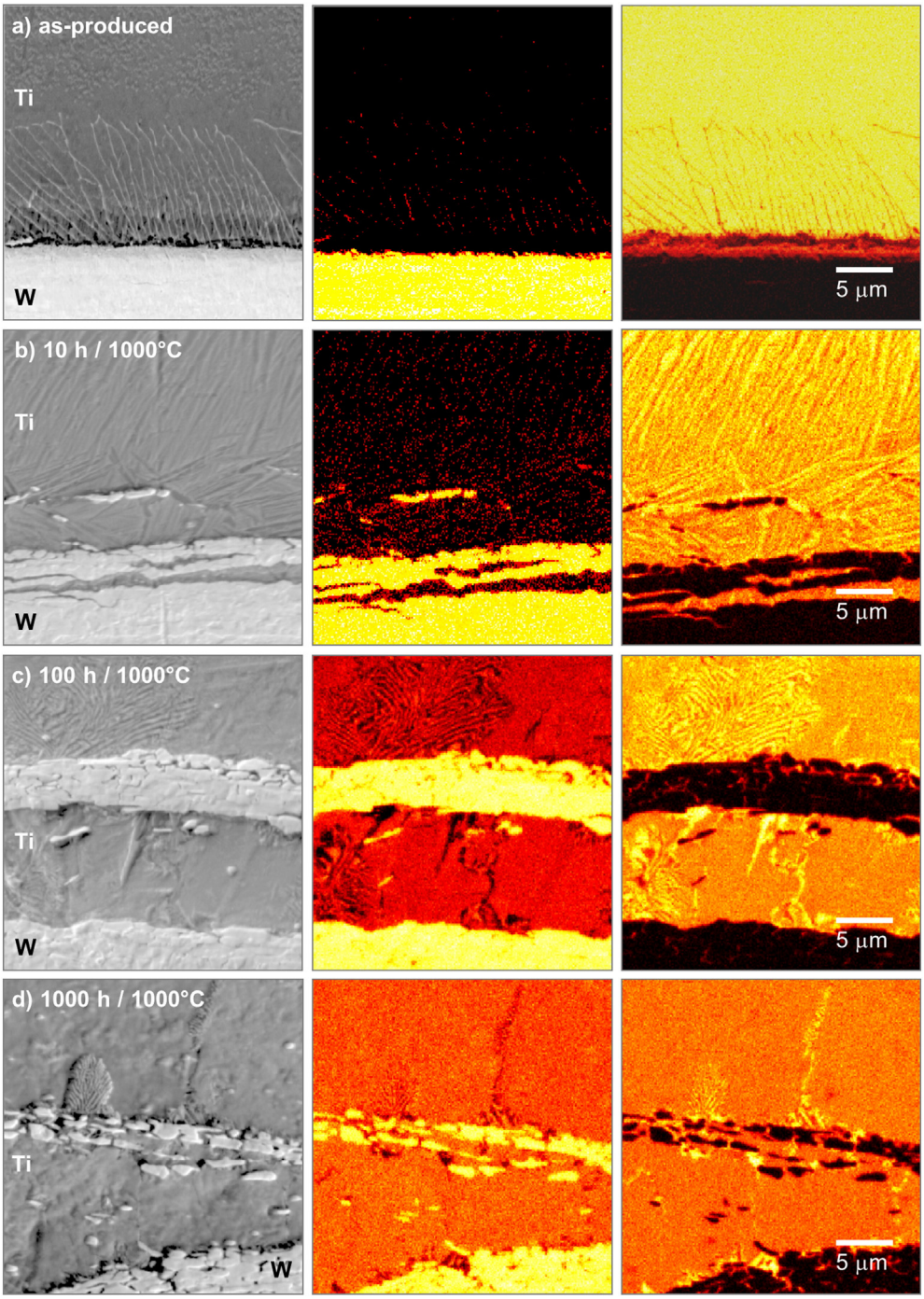

Fig. 7. AES analyses of tungsten titanium interfaces in different ageing conditions.

boundary bcc / (bcc + hcp) and its metastable extension in the phase diagram (Fig. 3). During the diffusion bonding the extension of the interdiffusion zone is less than 10 μm which is shown by the subse quently formed zone of Widmanstätten plates in Figs. 2 and 7a, respec tively. The width of the calculated diffusion profile (Fig. 5) is in the range of the experimentally observed zone.

In Fig. 7b the resulting microstructure is shown after the initial diffusion bonding process, a subsequent heating to 1000 °C for 10 h and furnace cooling (100 K/h). The titanium sheet has transformed throughout its whole width into a Widmanstätten structure consisting of thin plates with small precipitates at their boundaries. In comparison with the calculated diffusion profile (Fig. 5) the experimental range of the Widmanstätten structure seems to be too large. Furthermore, delamination effects are visible in the interface region between the titanium and tungsten sheet. This effect seems to be caused by grain boundary diffusion into the tungsten foils. As discussed above, the diffusion coefficients in W rich alloys are so small that under the given experimental conditions lattice diffusion can be neglected. However, the tungsten sheets have an ultrafine grained structure with a high density of grain boundaries which provides fast diffusion paths by means of grain boundary diffusion. As a result of the rolling process for manufacturing the tungsten foils, the tungsten grains are of a pancake like shape. Therefore, when titanium penetrates into the tungsten sheets mainly by grain boundary diffusion the shape of the grains causes a spread of titanium preferably parallel to the rolling direction. Then thin layers of Ti enriched alloy are formed which cause the delamination of packets consisting of several tungsten grains from the rest of the tungsten sheet. The delamination process increases the velocity of the mutual penetration of titanium and tungsten into each other. Therefore, the calculation of the interdiffusion process which considers only lattice diffusion results in shorter diffusion profiles and smaller displacements of the phase boundary than the observations in the experiments (Fig. 8, Table 2).

In Fig. 7c the interdiffusion zone between titanium and tungsten foils is shown after the initial diffusion bonding process, subsequent heating to 1000 °C for 100 h and furnace cooling. Here, the delamination process is even more pronounced. In addition, no more Widmanstätten structure is formed in the titanium foil. Instead, localised regions with eutectoid structure are present next to the tungsten foil or delaminated tungsten strips, respectively. Apart from the eutectoid regions major parts of the titanium foils seem to be homogeneous with no transforma tion structure. The measured tungsten concentration in the laminate, Fig. 9c, reveals that the alloy in the middle of the Ti foils contains about 6 at.% W which is still in the hypo monotectoid range (Table 3). Towards the interface to the tungsten foil the concentration rises to the value of 19% given by the phase diagram. Between these values a region is formed where the alloy is close to the monotectoid composition which transforms into a lamellar microstructure on cooling. In the phase diagram, Fig. 3, the phase boundaries of the equilibria hcp + bcc′ / bcc′ and bcc′ / bcc′ + bcc″ are extended by dotted lines into the metastable range below the monotectoid temperature. In the range between these dotted lines the formation of the lamellar monotectoid is possible. More precisely, if the interfacial energy of the lamellar monotectoid is taken into account, the dotted lines are displaced a bit towards lower temperatures.

Table 2
Movement of the interface: comparison between measurement and simulation.

Movement of the interface	Measurement	Simulation
As-produced	0 μm	0.2 μm
10 h/1000 °C	4.6 μm	1.1 μm
100 h/1000 °C	7 μm	3.3 μm
1000 h/1000 °C	10.7 μm	6.6 μm

However, the difference between the eutectoid and the monotectoid transformation has to be emphasized in this context. In Fig. 3 the exten sion of the line hcp + bcc′/bcc′ exists not more than about 20 K below the monotectoid temperature due to the presence of the miscibility gap. Therefore, monotectoid transformations are only possible while the sample passes through this narrow temperature range during cooling and accordingly the resulting lamellar regions are very small. Contrary to that, in a eutectoid system the matrix phase transforms into two new phases. The metastable extensions of their phase equilib ria exist at much lower temperatures below the eutectoid temperature and in this case considerable regions of the sample can transform in the eutectoid reaction.

Fig. 7d shows the interdiffusion zone of the diffusion bonded laminate after the additional heating for 1000 h at 1000 °C. In the interior of the titanium foil no transformation structure can be seen and the alloy seems to remain in the oversaturated bcc state. The Auger concentration profile (Fig. 9d) reveals here an almost constant hyper monotectoid level of about 13 at.% W in the titanium sheet. Furthermore, the delamination process of the tungsten foil in the vicinity of the interdiffusion zone is even more advanced (Fig. 7d). In the tungsten foil and in the delaminated strips the disintegration of these regions becomes visible as the Ti alloy infiltrates in between the tungsten grains by grain boundary diffusion. Occasionally, small regions next to tungsten strips reveal a lamellar transformation structure (Fig. 7d). Since these regions do not extend much into the adjacent Ti rich alloy a monotectiod reaction seems to be unlikely. Instead, a cellular precipitation mechanism can initiate the transformation on a tungsten grain boundary by forming a nucleus of hcp Ti. The regions next to the growing nucleus of hcp Ti become enriched in tungsten and they con vert into growing lamellae of bcc″ phase. Initially, the cellular pattern can spread over the thin grain boundary layer due to the enhanced grain boundary diffusion. Then the alternating stubs of hcp and bcc″ phase can grow into the adjacent Ti grain consisting of the matrix phase bcc′. This growth process is promoted by the enhanced grain boundary diffusion within the growth front between the matrix and the hcp and bcc″ lamellae, respectively.

5.2. Charpy impact properties and hardness

The results of the evolution of the Charpy impact properties and the evolution of the hardness will be discussed against the background of (i) the microstructural changes in the titanium interlayer, (ii) the

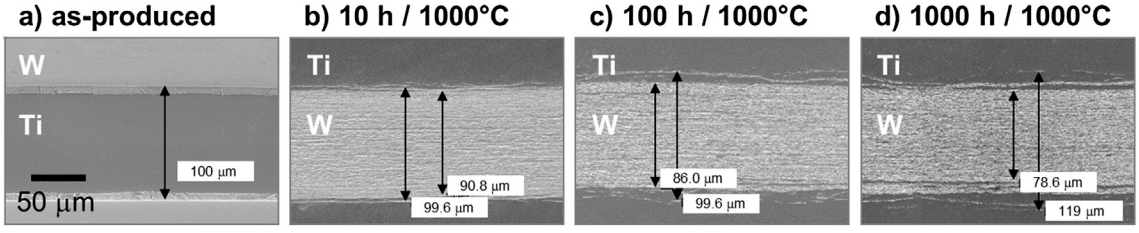

Fig. 8. SEM analyses of the movement of the interface. From left to right: (i) as-produced, (ii) annealed for 10 h at 1000 °C, (iii) annealed for 100 h at 1000 °C, and (iv) annealed for 1000 h at 1000 °C.

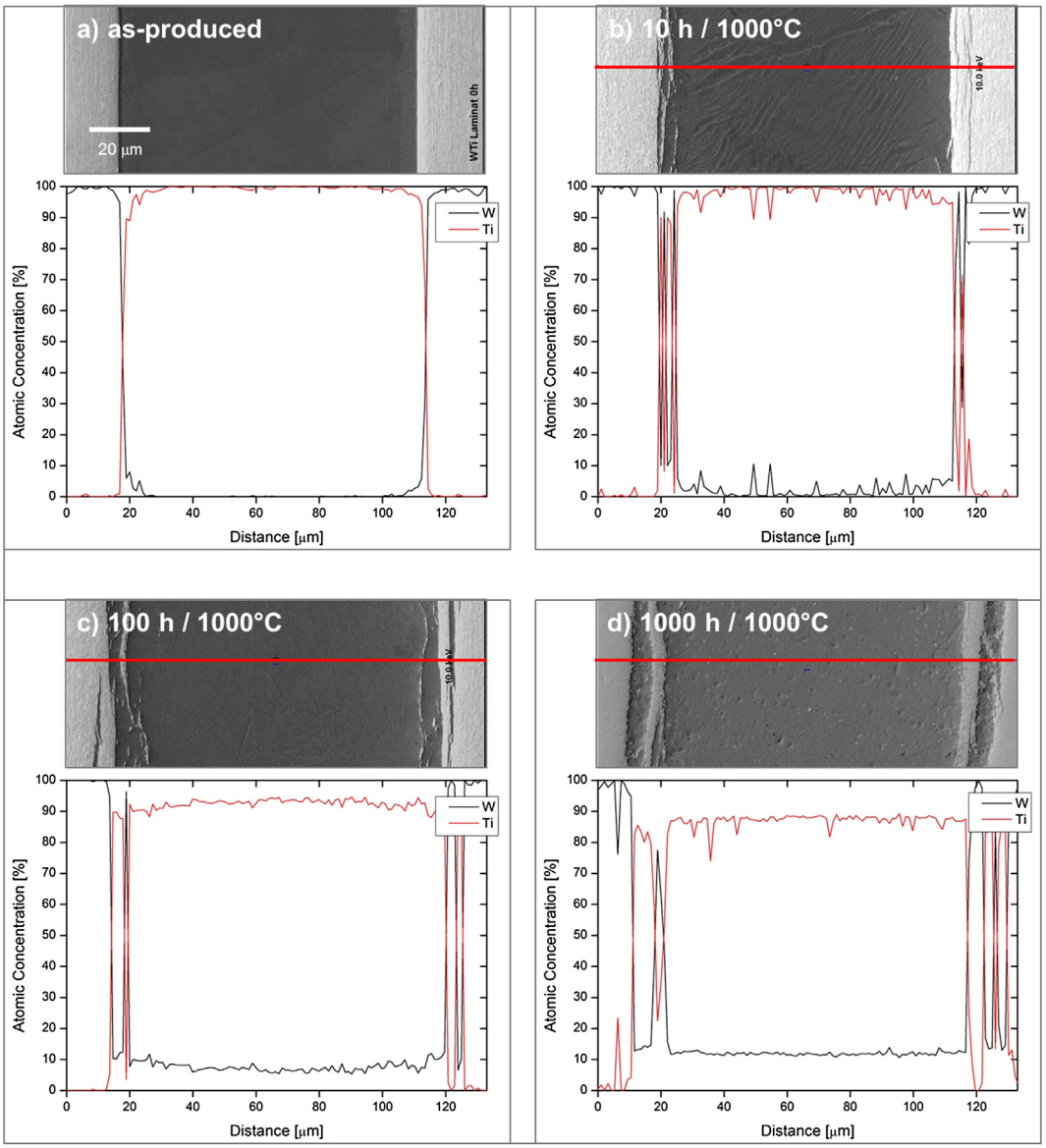

Fig. 9. AES line scans from tungsten to tungsten via the titanium interlayer. The axes show the atomic concentration in [%] over the distance in [µm]. The black lines represent the tungsten contents, the red lines the titanium contents.

microstructural changes in the tungsten layer, and (iii) the evolution of the W Ti interface after annealing. The four conditions, as produced and annealed at 1000 °C for 10 h, 100 h, and 1000 h, will be considered.

Fig. 10 displays the results of the Charpy impact tests of W Ti laminate samples with L S orientation. The lines plotted in grey are the results of benchmark experiments performed on technically pure (>99.97 wt.% W) tungsten plate material with a thickness of 4 mm (as received condition, L S orientation) and tungsten laminates produced by brazing with an eutectic silver copper brazing filler (as produced condition, L S orientation). For more details on the benchmark tests the reader is referred to Ref. [8,33].

Table 3
Diffusion profile: comparison between AES line scan and simulation.

Formed solid solution in Ti	Line scan, AES	Simulation
As-produced	<1 at.% W	0 at.% W
10 h/1000 °C	1 at.% W	0.4 at.% W
100 h/1000 °C	6 at.% W	4.4 at.% W
1000 h/1000 °C	13 at.% W	10.2 at.% W

In Fig. 10 the dissipated energy is plotted against the test temperature. In general, a discussion of how W Ti laminates in the L S orientation dissipate energy (plastic deformation of the tungsten layers, plastic deformation of the titanium interlayers, crack deflection and creation of surface) and of how residual stresses contribute to the crack behaviour of W Ti laminates would be appropriate and expected. However, the results of the Charpy impact tests can easily be summarised as the mechanical properties became significantly worse after annealing, so it has to be concluded that W Ti laminates with relatively thick titanium interlayers are not a candidate for high temperature applications at and beyond 1000 °C.

Nevertheless, an in depth understanding of the diffusion mechanisms of W Ti laminates can be derived from the hardness measurements.

The evolution of the hardness will be discussed for both the titanium interlayer and the tungsten layer. The Vickers hardness measured was HV0.1. For each of the four material conditions at least 12 hardness indents were used and the arithmetical means of the measurements with the root mean square deviation are reported.

Fig. 11 displays the results of the hardness measurements where the hardness HV0.1 is plotted against the annealing time. The discussion of

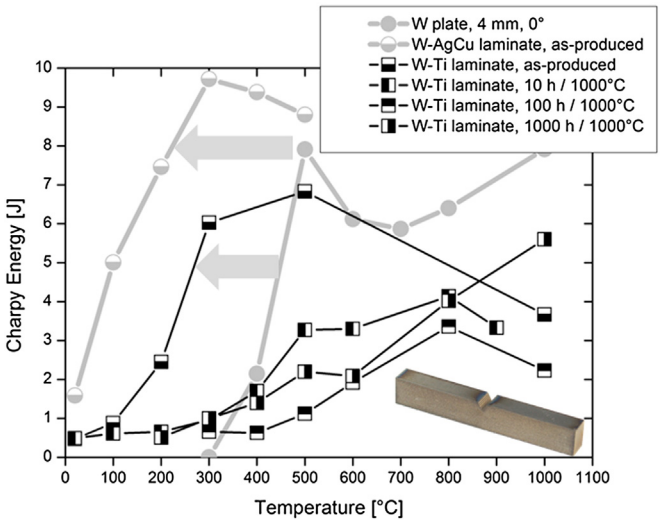

Fig. 10. Results of the Charpy impact tests. The dissipated energy is plotted against the test temperature. All samples were oriented in L–S direction.

the evolution of the hardness in the titanium interlayer is straightfor ward. The increase of the hardness in the titanium interlayer with annealing time can easily be attributed to solid solution hardening. This interpretation seems to be feasible as the simulation of diffusion showed that diffusion of tungsten into titanium has to be considered (Figs. 4, 5) and the AES line scans showed the increase of tungsten in the titanium interlayer with annealing time (Fig. 9, Table 3).

The interpretation of the evolution of the hardness in the tungsten layer is more complex. For the sake of comparison Fig. 11 also displays the hardness HV0.1 of the 100 μm tungsten foil in its as received condition [25] as well as the hardness HV0.1 of 100 μm tungsten foil after annealing for 1 h at 2700 °C [25] and the hardness HV0.1 of a tungsten single crystal (grown on a Pintch wire, with (100) as plane of indentation) [2]. Additional hardness values can be found in Table 4. As the tungsten foil used for the synthesis of the W Ti laminate has a sharp rotated cube texture both in the as received and in the annealed condition [25], the comparison of the hardness of the tungsten layer of a W Ti laminate with the hardness of a tungsten single crystal with an indentation plane of (110) seems to be reasonable.

From Fig. 11 and Table 4 it can be seen that during the synthesis of the W Ti laminate, the microstructure of the tungsten foil slightly changes. This might be attributed to recovery processes such as

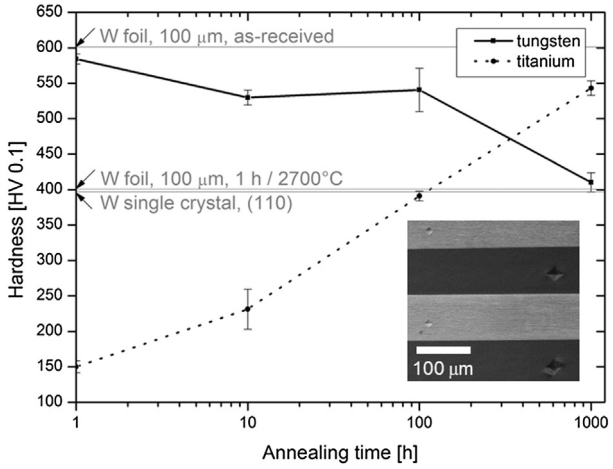

Fig. 11. Vickers hardness HV0.1 plotted against the annealing time. The W–Ti laminates were produced by diffusion bonding at 900 °C for 1 h and then annealed at 1000 °C for 10 h, 100 h, and 1000 h.

dislocation annihilation, dislocation rearrangement, and sub grain growth. Considering the results of the Charpy impact tests, these recov ery processes during the synthesis of the W Ti laminates might be the reason for the shift of the BDTT to higher temperature compared with the BDTT of tungsten laminates made by brazing with an eutectic silver copper brazing filler, for which the joining parameters were 800 °C for 5 min. According to this finding one might assume that the BDT of tungsten laminates in general and of UFG tungsten foils in particular sensitively depends on microstructural features such as point and line defects.

During annealing of the W Ti laminates at 1000 °C for 10 h, 100 h, and 1000 h, the hardness of the tungsten layer decreases significantly. This results in a hardness value of 410 HV0.1 for a W Ti laminate annealed for 1000 h at 1000 °C. This value is in the same range as the hardness value of a coarse grained tungsten foil (100 μm, annealed for 1 h at 2700 °C) and even that of a tungsten single crystal (grown on a Pintch wire, with (110) as plane of indentation). Taking this comparison into account the tungsten layers of the W Ti laminate annealed for 1000 h at 1000 °C should display a very coarse grained microstructure. However, Fig. 8 shows that this is not the case the tungsten layers still look ultrafine grained. The question is: why?

From the diffusion data from Fig. 4 it can be seen that there is almost no diffusion of titanium into tungsten so a solid solution hardening/softening by the formation of a W Ti solid solution can be excluded from the discussion. This leaves only recovery processes (dislocation annihilation, dislocation rearrangement, and sub grain growth), primary recrystallisation (movement of high angle grain boundaries), or secondary recrystallisation (selective grain growth). Consequently, the evolution of the hardness value can only be attrib uted to changes in the dislocation structure (recovery) and changes in the grain size (recrystallisation).

From the images of the evolution of the tungsten microstructure in Fig. 8 one has to point out that the grain size does not change signifi cantly during annealing. Consequently, recrystallisation must also be excluded from the discussion. This leaves recovery only. This suggests that the evolution of the hardness of the tungsten layer during anneal ing depends on recovery processes only. We think that that explanation is not convincing and that there is a much more reasonable explanation, which is as follows.

From the simulation of diffusion in W Ti laminates it can be seen that tungsten diffuses into the titanium interlayer whereas the opposite process of titanium entering into the tungsten layer is not visible (Fig. 5). It is important to note at this point that the simulation considers lattice diffusion only, and that grain boundary diffusion is not considered in the numerical analyses. However, from the AES analyses in Fig. 7 it can be seen that there is a significant grain boundary diffusion of titanium along the tungsten grain boundaries. Thus grain boundary diffusion must be considered in the discussion of the mechanisms of the evolution of the microstructure of the annealed W Ti laminates. It is well known that grain boundaries provide the most prominent high diffusivity paths and that grain boundary diffusion in metals is typically four to six orders of magnitude faster than lattice diffusion [34]. Given these facts we provide a new line of argument.

Considering the diffusion of titanium into the tungsten layer along tungsten grain boundaries, one might assume that after annealing for several hours at 1000 °C most of the tungsten grain boundaries would be covered with titanium. This might have considerable consequences for both the recrystallisation behaviour and the hardness of the tungsten layer. Due to the fact that most grain boundaries are wetted with titanium, the recrystallisation mechanisms might look similar to those of potassium (K) doped tungsten. In a properly processed potassi um doped tungsten material, the potassium bubbles are aligned in rows and act as barriers to grain boundary migration. It is likely that if the tungsten grain boundaries are covered with titanium, the traces of titanium might act as barriers that impede the grain boundary migration and thus suppress grain growth. Furthermore, an increase

Table 4
Comparison of the hardness HV0.1 of the tungsten layer of a W–Ti laminate with the hardness of tungsten foil, 100 μm [25], and tungsten single crystals (grown on a Pintch wire) [2].

W material	W–Ti laminate, as-produced	W–Ti laminate, 1000 h at 1000 °C	W foil, 100 μm, as-received	W foil, 100 μm, annealed 1 h at 2700 °C	W single crystal, plane of indentation: (100)	W single crystal, plane of indentation: (110)	W single crystal, plane of indentation: (111)
Hardness, HV0.1	585	410	602	405	360	395	408

of the content of titanium at the tungsten grain boundaries will also lead to a decrease of the hardness of the tungsten layer. Therefore the low hardness value of 410 HV0.1, measured on the tungsten layer of a W Ti laminate annealed for 1000 h at 1000 °C, could well be caused by a high content of titanium in the tungsten layer, whereas the titanium is preferentially located at the tungsten grain boundaries.

6. Conclusion

It is intended that tungsten laminates made of UFG tungsten foil enhance the upper end of the temperature window of structural high temperature materials. Furthermore, pipes made of UFG tungsten foil might enable innovative high temperature energy conversion systems to improve their performance.

In this paper we analysed and discussed the ageing behaviour of tungsten laminates produced by diffusion bonding with a titanium interlayer. The evolution of the mechanical properties (Charpy impact, hardness) and the evolution of the microstructure during annealing at 1000 °C for 10 h, 100 h, and 1000 h in vacuum have been very well studied.

The calculated W Ti phase diagram, as well as the calculated interdiffusion coefficients and interdiffusion profiles, was significantly related to the understanding of the evolution of the W Ti interface. The comparison of the AES and SEM analyses with the simulated diffusion data provided an in depth understanding of the diffusion mechanisms and of the evolution of the microstructure.

One of the main objectives of this work was to assess whether or not W Ti laminates are a candidate for structural high temperature applica tions. Our results clearly identified that W Ti laminates are inappropriate for structural applications at 1000 °C, as the Charpy impact properties deteriorate through annealing. However, in all fairness, it has to be said that the Charpy impact properties of the annealed W Ti laminates were not benchmarked against annealed pure tungsten plate material. These benchmark experiments still need to be carried out.

The in depth understanding of the diffusion mechanisms of W Ti laminates will advance several research fields (Fig. 12).

- One promising way to produce UFG tungsten bulk material consists in the diffusion bonding of several layers of UFG tungsten foil, preferably without any interlayer at all (alternative method to high pressure torsion (HPT) [35,36] or equal channel angular pressing (ECAP) [37 39]). In order to reduce the bonding temperature and bonding time, the activation of the tungsten foil surfaces by several atom layers of titanium is an option. It is very likely that the joining at 900 °C is feasible and that the ageing behaviour can be explained by the diffusion mechanisms identified in this study.
- In order to determine fracture mechanical properties of tungsten semi finished products in specific orientations, e.g. the fracture toughness of tungsten foils in S L orientation, it is common practice to extend the test samples. Such an extension can be realised by brazing with a copper based (tungsten single crystal, 2 min/1110 °C [40]) or nickel based (tungsten rod material, R L orientation, 30 min/1050 °C [41]) brazing filler.

The requirements for the joining process of the extension of the test samples are as follows: (i) in order not to change the microstructure of the test sample, the bonding temperature must be well below the recrystallisation temperature, (ii) in order to determine the BDTT and to obtain reliable K_{IC} values, the joint must have high strength at temperatures beyond the BDTT, and (iii) the crack propagation path and the plastic zone around the crack tip must be free of any diffused elements of the joining interlayer. These requirements can be met by extending the samples by diffusion boning at 900 °C with a titanium interlayer.

It is particularly samples in S L orientation that will contribute to the question of the anisotropy of the shift of the BDT to lower temperatures through cold rolling. Furthermore, it is the samples in S L orientation that can elucidate the impact of former sinter pores, impurities on the grain boundaries, microspores, and crystallographic texture on the fracture behaviour of tungsten [42,43]. In this study we showed what a promising sample preparation might look like.

UFG tungsten foils have exceptional mechanical properties. Through innovative nanoengineering, like the synthesis of tungsten foil laminates, UFG tungsten bulk materials can be produced that retain the ductility of the tungsten foil. These materials might have the potential to be used for structural applications and thus open a new era for tungsten.

Acknowledgements

This work has been carried out within the framework of the EUROfusion Consortium and has received funding from the Euratom

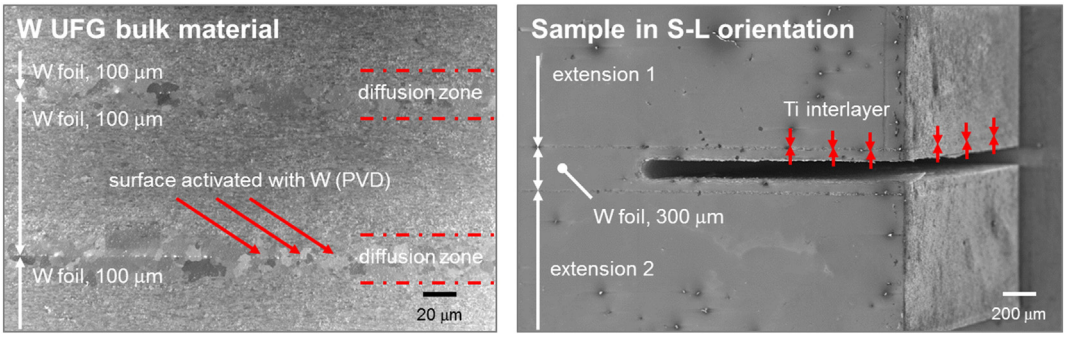

Fig. 12. The elucidation of the diffusion mechanisms of W–Ti laminates will advance other research fields such as the production of UFG bulk material (left) or the synthesis of advanced fracture toughness test samples (right).

Research and Training Programme 2014 2018 under grant agreement No 633053. The views and opinions expressed herein do not necessar ily reflect those of the European Commission. The authors are grateful to all their colleges at the Karlsruhe Institute of Technology (in alpha betical order: S. Baumgärtner, D. Bolich, S. Bonk, Dr D. Cupid, B. Dafferner, K. Erbes, M. D. Hoffmann, U. Jäntsch, Dr M. Klimenkov, A.A.N. Németh, and J. Scherbarth) for their support and valuable con tribution. Particular thanks go to Prof. H. J. Seifert, and Prof. A. Möslang. The support of the tungsten supplier, PLANSEE SE, Reutte/ Austria, is gratefully acknowledged.

References

[1] C.R. Hammond, The Elements, in Handbook of Chemistry and Physics, 89st ed. CRC press, 2008.
[2] E. Lassner, W.D. Schubert, Tungsten — Properties, Chemistry, Technology of the Element, Alloys, and Chemical Compounds, Springer, Berlin, 1999.
[3] Q. Wei, L.J. Kecskes, Mater Sci. Eng. A Struct. 491 (2008) 62.
[4] R. Pippan, presented at W conference, organized by Odette GR, UCLA, Santa Barbara, USA, February 2011.
[5] J. Reiser, M. Rieth, A. Möslang, et al., Tungsten (W) laminate pipes for innovative high temperature energy conversion systems, Adv. Eng. Mater. 17 (4) (2015) 491–501.
[6] A.A.N. Németh, J. Reiser, D.E.J. Armstrong, M. Rieth, Int. J. Refract. Met. Hard 50 (2015) 9.
[7] Annual Book of ASTM StandardsStandard Test Method for Plane-Strain Fracture Toughness of Metallic Materials (ASTM E 399–90), vol. 03.01, American Society for Testing and Materials, 1997.
[8] J. Reiser, M. Rieth, B. Dafferner, A. Hoffmann, J. Nucl. Mater. 423 (2012) 1.
[9] Z. Zhong, T. Hinoki, T. Nozawa, Y.H. Park, A. Kohyama, J. Alloys Compd. 489 (2010) 545.
[10] H. Choe, S.M. Abkowitz, S. Abkowitz, D.C. Dunand, J. Alloys Compd. 390 (2005) 62.
[11] R. Lison, Schweißen und Löten von Sondermetallen und ihren Legierungen, Deutscher Verlag für Schweißtechnik, Düsseldorf, 1996.
[12] R. Lison, Wege zum Stoffschluß über Schweiß- und Lötprozesse, DSV-Verlag, Düsseldorf, 1998.
[13] Landolt-Börnstein, Springer Materials, New Series IV/5, 2010.
[14] S.V. Nagender Naidu, Rao R. Rama, Phase Diagrams of Binary Tungsten Alloys, India Institute of Metals, Calcutta, 1991.
[15] E. Arzt, Acta Mater. 46 (1998) 5611.
[16] W.D. Nix, Metall. Trans. A 20A (1989) 2217.
[17] A. Misra, J.P. Hirth, H. Kung, Philos. Mag. A 82 (2002) 2935.
[18] S.B. Lee, J.E. LeDonne, S.C.V. Lim, I.J. Beyerlein, A.D. Rollett, Acta Mater. 60 (2012) 1747.
[19] I.J. Beyerlein, N.A. Mara, J.S. Carpenter, et al., J. Mater. Res. 28 (2013) 1799.
[20] Y.P. Li, G.P. Zhang, Z.G. Wang, Adv. Mater. Res. 41 (2008) 3.
[21] S. Shao, H.M. Zbib, I.N. Mastorakos, D.F. Bahr, J. Appl. Phys. 112 (2012) 044307.
[22] J. Reiser, M. Rieth, A. Möslang, B. Dafferner, A. Hoffmann, X. Yi, D.E.J. Armstrong, J. Nucl. Mater. 434 (2013) 357.
[23] O. Kubaschewski, B.E. Hopkins, J. Less-Common Met. 2 (1960) 172.
[24] X.J. Yuan, G.M. Sheng, B. Qin, W.Z. Huang, B. Zhou, Mater. Charact. 59 (2008) 930.
[25] J. Reiser, M. Rieth, B. Dafferner, A. Hoffmann, X. Yi, D.E.J. Armstrong, J. Nucl. Mater. 424 (2012) 197.
[26] M. Rieth, A. Hoffmann, Int. J. Refract. Met. Hard 28 (2010) 679.
[27] N. Saunders, in: I. Ansara, A.T. Dinsdale, M.H. Rand (Eds.),COST 507, Thermochemical Database for Light Metal Alloys, vol. 2 1998, pp. 299–302 (Luxembourg).
[28] A. Borgenstam, A. Engström, L. Höglund, J. Ågren, J. Phase Equilib. 21 (2000) 269.
[29] A.E. Pontau, D. Lazarus, Phys. Rev. B 22B (1979) 4027.
[30] S.M. Klotsman, G.N. Tatarinova, A.N. Timofeev, Defect Diffus. Forum 319 (2011) 1.
[31] N.K. Arkhipova, S.M. Klotsman, YaA Rabovskiy, A.N. Timofeyev, Phys. Met. Metallogr. 43 (1977) 88.
[32] L.V. Pavlinov, Phys. Met. Metallogr. 24 (1967) 70.
[33] J. Reiser, M. Rieth, B. Dafferner, A. Hoffmann, J. Nucl. Mater. 442 (2013) S204.
[34] H. Mehrer, Diffusion in Solids, Springer, Berlin, 2007.
[35] M. Faleschini, H. Kreuzer, D. Kiener, R. Pippan, J. Nucl. Mater. 367 (2007) 800.
[36] Q. Wei, H.T. Zhang, B.E. Schuster, K.T. Ramesh, R.Z. Valiev, L.J. Kecskes, R.J. Dowding, L. Magness, K. Cho, Acta Mater. 54 (2006) 4079.
[37] Q. Wei, T. Jiao, K.T. Ramesh, E. Ma, L.J. Kecskes, L. Magness, R. Dowding, V.U. Kazykhanov, R.Z. Valiev, Acta Mater. 54 (2006) 77.
[38] L.J. Kecskes, K.C. Cho, R.J. Dowding, B.E. Schuster, R.Z. Valiev, Q. Wei, Mater. Sci. Eng. A 467 (2007) 33.
[39] A.V. Ganeev, R.K. Islamgaliev, R.Z. Valiev, Phys. Met. Metallogr. 115 (2014) 139.
[40] J. Riedle, Bruchwiderstand in Wolfram-Einkristallen: Einfluss der kristallographischen Orientierung, der Temperatur und der Lastrate, Reihe 18, Nr.184, VDI Verlag, Düsseldorf, 1990.
[41] D. Rupp, Bruch und Spröd-duktil-Übergang in polykristallinem Wolfram: Einfluss von Mikrostruktur und Lastrate(Dissertation) Karlsruhe Institute of Technology, 2010.
[42] B. Gludovatz, S. Wurster, T. Weingartner, A. Hoffmann, R. Pippan, Philos. Mag. 91 (2011) 1.
[43] A. Hoffmann, I. Wesemann, Int. J. Powder Metall. 47 (2011) 1.